Title
Heat Transfer with Superalloy Finned Tubes for Supercritical CO2 Heat Exchangers

Author
Murley, Bryce Dutro

Publication Date
2022

Peer reviewed|Thesis/dissertation

UNIVERSITY OF CALIFORNIA
Los Angeles

Heat Transfer with Superalloy Finned Tubes for Supercritical CO_2 Heat Exchangers

A thesis submitted in partial satisfaction
of the requirements for the degree
Master of Science in Mechanical Engineering

by

Bryce Dutro Murley

2022

ABSTRACT OF THE THESIS

Heat Transfer with Superalloy Finned Tubes
for Supercritical CO_2 Heat Exchangers

by

Bryce Dutro Murley
Master of Science in Mechanical Engineering
University of California, Los Angeles, 2022
Professor Timothy Fisher, Chair

Supercritical CO_2 (sCO_2) Brayton cycles are promising power cycles due to their high theoretical efficiencies and power densities. However, these cycles require the development of highly compact and effective sCO_2 heat exchangers in order to achieve these potential benefits. This study experimentally characterizes the heat transfer performance of superalloy finned tubes in sCO_2 cross-flow for eventual use in shell and tube heat exchangers. Two finned tube designs, with disc and parabolic fins, were tested against a bare tube in cross-flow with with Reynolds numbers ranging from $3{,}500 \leq Re \leq 8{,}000$. Both finned tube designs significantly outperformed the bare tube, and fins were shown to increase the Nusselt number of the tube by more than double in every case. The disc-finned tubes achieved higher overall heat transfer, but the parabolic fins are shown to have higher fin efficiency in every case. Lastly, this study compares the experimental results with correlations for Nusselt number and fin efficiency developed in previous studies.

The thesis of Bryce Dutro Murley is approved.

Xiaochun Li

Portonovo Ayyaswamy

Timothy Fisher, Committee Chair

University of California, Los Angeles

2022

TABLE OF CONTENTS

List of Figures

List of Tables

ACKNOWLEDGMENTS

I would like to express my deepest gratitude to Dr. Timothy Fisher and to Dr. Kaiyuan Jin for their mentorship and support throughout this process. This thesis would not have been possible without their constant guidance and knowledge. I would also like to thank Dr. Akshay Krishna, Danny Chmaytelli, Nicholas Wolff, and Zachary Wong for their collaboration and assistance with the project.

CHAPTER 1

Introduction

1.1 Motivation

As the world's demand for energy increases and concern over the impacts of climate change grows, it is becoming increasingly important to improve energy conversion efficiency. New thermal power cycles are being developed to more efficiently convert energy from conventional thermal sources such as fossil fuels and geothermal energy as well as from newer, low-emission sources such as Generation IV nuclear and concentrated solar thermal [1]. Supercritical carbon dioxide (sCO_2) Brayton cycles are particularly promising due to their potential for high thermal efficiency, small system footprints, stability, and wide range of applications. They achieve high thermal efficiency by operating at high temperatures and because the working fluid is nearly incompressible throughout the cycle, meaning that less energy is required for compression. A smaller overall system size is possible because sCO_2 remains dense throughout the cycle which allows for higher volumetric power density. sCO_2 is also less corrosive than most other working fluids in the supercritical state, is non-toxic, and is supercritical over a large range of operating temperatures at feasible working pressures [2]. These benefits make sCO_2 Brayton cycles more attractive than traditional steam Rankine cycles for a wide range of energy conversion applications.

Although promising, sCO_2 Brayton cycles require further development on both the cycle components and the optimal cycle layout. Each component of the sCO_2 Brayton cycle must be developed for a new working fluid and to withstand high operating temperatures and

pressures [12]. This includes the development and characterization of new materials, such as nickel superalloys [3], that can withstand the cycle conditions. Recent studies have shown that various optimized layouts can be utilized depending on the specific application of the cycle. A key aspect of any high efficiency configuration is the use of multiple recuperators to recover process heat from the relatively high temperature fluid at the turbine outlet. Therefore, highly compact and effective heat exchangers (HXs) are required for use in the cycle because they make up a large portion of the overall system cost, efficiency, and footprint [4].

Shell and tube heat exchangers (STHX) are one of the most commonly used heat exchanger designs for high temperature and high pressure applications. These heat exchangers consist of parallel tubes connected by a header inside of a shell. One fluid flows inside of the tubes, while the other fluid flows inside the shell to heat or cool the tube-side flow. Typically, the shell contains baffles that guide the shell-side fluid to flow normal to the tubes and allow multiple passes of shell-side flow over the tube bundle to increase heat transfer effectiveness. SHTXs have been proposed for use as recuperators, cooling HXs, and primary HXs in sCO_2 Brayton cycles. However, further work is required to characterize STHXs for the unique operating conditions of sCO_2 cycles. Maximizing the overall heat transfer effectiveness and compactness of the STHX, while minimizing its overall pressure drop, is critical for developing an economically viable sCO_2 heat exchanger. A common way to improve the effectiveness and compactness of STHXs is by using annular finned tubes. Fins increase the heat transfer surface area without increasing the total volume of the STHX, but they also increase pressure drop and overall HX weight. Therefore, there is great interest in finding optimal fin geometries for heat exchanger tubes [5].

This study experimentally characterizes the heat transfer performance of Haynes-282 finned tubes in supercritical CO_2 cross flow. A bare tube, disc-finned tube, and novel parabolic-finned tube are tested as single tubes in cross-flow over a range of external flow temperatures and Reynolds numbers. This study aims to evaluate various fin geometries for

their effect on overall STHX performance.

1.2 Related Work

Previous studies by Chen et al. [6], Watel et al. [7], and Hu et al. [8] have numerically and experimentally characterized heat transfer with single annular finned tubes for different fin geometries in forced convection cross-flow. Typically these studies use air as the external flow fluid and attempt to provide a general correlation for the heat transfer coefficient and fin efficiency based on the tube geometry and flow conditions.

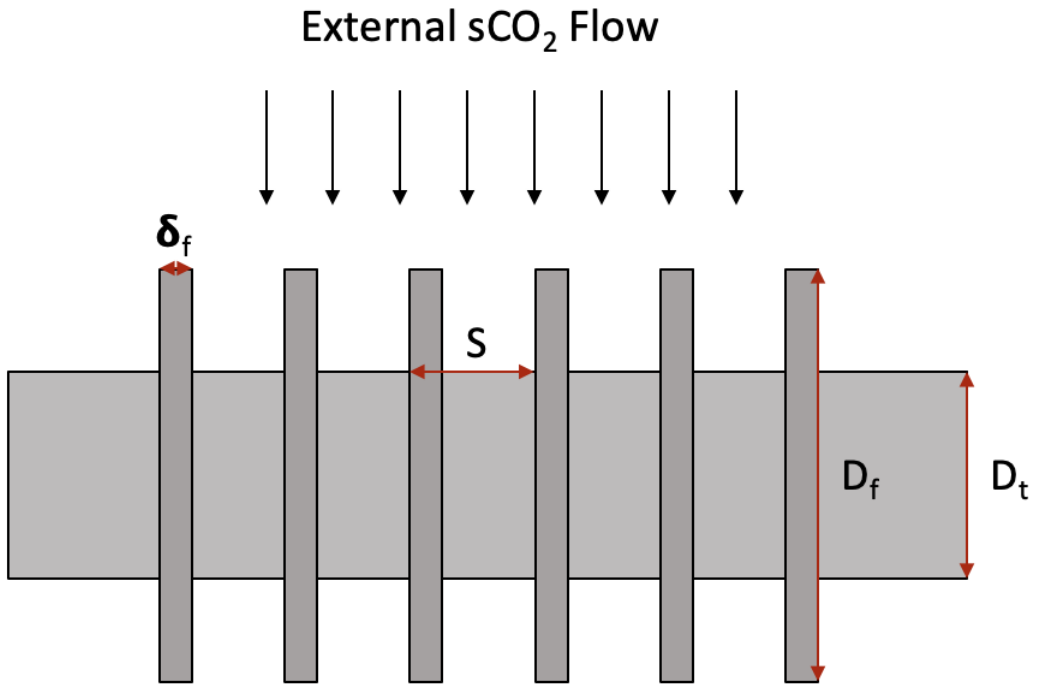

Figure 1.1: Schematic of a finned tube in cross-flow.

External flow over a cylinder has been well studied, and several correlations have been developed relating the Nusselt number to the Reynolds number and Prandtl number of the

fluid [9]. These dimensionless parameters are defined as

$$Re = \frac{uD_t}{\nu} \tag{1.1}$$

$$Pr = \frac{\nu}{\alpha} \tag{1.2}$$

$$Nu = \frac{hD_t}{k} \tag{1.3}$$

where u is the fluid velocity in the cross-flow direction, ν is the dynamic viscosity, α is the thermal diffusivity, h is the convective heat transfer coefficient, and k is the thermal conductivity of the fluid. For this study, the conduction through the fins and the convection on the fin surfaces are of particular interest. This is generally a much more complex problem due to the fin geometries and interactions between the boundary layers of the fins and tube surface. To fully characterize the fin, the temperature profile and the convective heat transfer coefficient must be solved as a function of the radial and axial position. Assuming constant thermal properties, steady state, and an insulated tip, the 2-D heat conduction equation for the fin on a one-finned annular finned tube heat exchanger can be expressed as:

$$\frac{\partial^2 T}{\partial r^2} + \frac{1}{r}\frac{\partial T}{\partial r} + \frac{1}{r^2}\frac{\partial^2 T}{\partial \theta^2} = \frac{2h(r,\theta)}{k_f \delta}(T - T_\infty) \tag{1.4}$$

for $\mathrm{R}_i \leq \mathrm{r} \leq \mathrm{R}_o$ and $0 \leq \theta \leq 2\pi$ [6]. R_i is the tube radius and R_o is the fin radius. The boundary conditions are given by:

$$\frac{\partial T(r,0)}{\partial \theta} = \frac{\partial T(r,2\pi)}{\partial \theta} \tag{1.5}$$

$$T(r,0) = T(r,2\pi) \tag{1.6}$$

$$T(R_i,\theta) = T_o \tag{1.7}$$

$$\frac{\partial T(r,\theta)}{\partial r} = 0 \tag{1.8}$$

In the governing equation (1.4), the convection term $h(r,\theta)$ on the right hand side is typically unknown, since it is a function of both the radial and axial location on the fin as well as complex flow physics. Single tube heat transfer studies generally aim to quantify the average heat transfer coefficient empirically as a function of tube geometry and flow conditions, as this will characterize the system level heat transfer performance. Chen et al. estimated heat transfer characteristics of annular finned tubes in forced convection cross flow of air using a finite difference method in conjunction with the least-squares scheme and experimental measurements. The researchers divided the fins into sub-fin regions and presented difference equations for nodes at the interfaces of the regions based on the two-dimensional conduction equation. To estimate the heat transfer coefficients, they used experimental measurements of temperature at six sub-fin region locations. This allowed them to estimate heat transfer coefficients by using a least-squares minimization technique to minimize the sum of the squares of the deviations between the calculated and measured temperatures at the measured locations. The local calculations for heat transfer coefficient and heat transfer rate were used to predict the average heat transfer coefficient of the entire fin and the overall fin efficiency. The study was conducted for fin spacing ranging from $0.005\text{m} \leq S \leq 0.018\text{m}$ and Reynolds numbers ranging from $1{,}550 \leq Re \leq 7{,}760$. Ultimately, the study presented correlations for average Nusselt number and fin efficiency as a function of the Reynolds number and finned tube geometry. The resulting correlations are

$$Nu_d^{iso} = 16.5185 d_o[(2.54\frac{\delta_f}{S} + 0.6925)Re_d(1 - \frac{K^*}{(S/D_t)^b(Re_d)^{0.07}})]^{0.55}(\frac{1}{V_{air}})^{0.123} \tag{1.9}$$

$$\eta_f = (0.208\frac{\delta_f}{S} + 1)[0.40783 - 4.17947 \times 10^{-5} Re_d + 2.598 \times 10^{-9}(Re_d)^2](1 + \frac{25.61}{(S/D_t)^{0.55} Re_d}) \tag{1.10}$$

where b = 0.55 and K* = 0.36 for the geometry in this study. Chen et al. also provided key insights into the heat transfer physics of the finned tube in cross flow. Their results showed that the local heat transfer coefficients were consistently higher for upstream sub-fin regions due to low-performing wake regions in the downstream flow – close to 4 times higher for the the two front-most sub-regions compared to the two furthest in the wake region. They showed that the average heat transfer coefficient increases with increasing air speed and fin spacing, while the fin efficiency decreased with increasing air speed and was not very sensitive to fin spacing [6].

Watel et al. [7] conducted a similar experimental study in which they evaluated convective heat transfer from fins using infrared thermography and Particle Image Velocimetry (PIV). By measuring the fin surface temperatures with thermography, they were able to calculate heat transfer coefficient corresponding to Reynolds numbers ranging from 2,550 $\leq Re \leq$ 42,000 and dimensionless fin spacing ($S' = \frac{S}{D_t}$ from $0.034 \leq S' \leq 0.69$). PIV was used to obtain measurements of the flow field between the fin surfaces. The researchers developed a correlation for Nusselt number as a function of the fin spacing and Reynolds number and compared it to the results from other studies . Watel et al.'s correlation is given by

$$Nu_d^{iso} = 0.446[(\frac{\delta_f}{S} + 1)(1 - \frac{K^*}{(S/d_o)^b (Re_d)^{0.07}})]^{0.55} Re^{0.55} \tag{1.11}$$

where b and K* are the same as above. Watel et al.'s results showed that Nusselt number increases with increasing Re and increasing fin spacing. They proposed that this is the result of the interacting boundary layers in between the fins which results in higher kinetic energy loss due to friction on the fin walls. From the PIV results, they also observed that the boundary layer thickness between the fins decreases with increasing Re. This leads to a decrease in interaction between the boundary layers and thus helps to explain why the Nusselt number trends towards that of the single fin limiting case ($S' = \infty$) at high Re. The study also suggests the use of von Karman's equation that approximates boundary layer thickness at the tail edge of a fin in order to predict the fin spacing at which the boundary

layers in between fins are thin enough to not interact [7].

Hu et al. [8] used a naphthalene sublimation technique to study mass transfer on a single row of annular finned tubes in cross-flow in order to infer local effects on overall heat transfer fin efficiency. They used a wind tunnel to conduct the experiments on a single row of five annular finned tubes with $D_f = 76.2mm$ and $D_t = 38.1mm$, for Reynolds numbers ranging from 3,300 $\leq Re \leq$ 12,000. Using the measured sublimation depth on the finned tubes, as well as temperature and pressure measurements, the researchers were able to calculate the local and average Sherwood numbers. By invoking the heat and mass analogy, they inferred the local and average Nusselt numbers and heat transfer coefficients. The obtained heat transfer coefficients were used to calculate fin efficiency and the results were compared to the Gardner fin efficiency [10, 11].

The study by Hu et al. provides interesting results for local heat and mass transfer and the nature of the flow around the fins. For moderate Re $\leq$ 9,000, mass transfer is highest near the front of the fin and the back of the fin. This is likely due to boundary layer development, and the higher values at the back may be due to a weak intermittent root vortex. The fins also exhibited peaks in Sherwood number at 120 and 240 degrees from the front of the fin in the axial direction, and a region with low Sherwood number in between those peaks. The study also finds that fin efficiency differs from the Gardner efficiency by up to 18% when local heat transfer behavior is included, and proposes parameters that may be useful for characterizing deviation from the Gardner efficiency with fin geometries alone [8, 11].

In tube bundles, the wake from upstream tubes affects the heat transfer performance of downstream tubes. Studies that characterize tube bundles account for this behavior by developing correlations for the average heat transfer coefficients as a function of the tube and tube bundle geometry in addition to the upstream flow characteristics. Ultimately, the goal of this study is to use the fin designs in tube banks as part of heat exchangers, and so correlating the experimental results to tube bundle models is a critical next step. Previous work on the characterization of finned tube bundles and STHXs include work by

Kays and London [12], Biery et al. [13], and Krishna et al. [5, 14]. The book by Kays and London on compact heat exchangers presents a large set of experimental tube bundle data and correlations. The text includes a wide variety of tube geometries and tube bundle configurations, and correlations for Nusselt number and friction factor as a function of the Reynolds number. Importantly, the authors define a key geometric parameter called the hydraulic diameter (D_h) that characterizes the tube bundle and is used in several other studies for calculating the Reynolds number

$$D_h = 2\frac{A_c P_l}{A_{HT}} \tag{1.12}$$

where A_c is the flow cross-section area, also called the free flow area, which is the planar area between the two closest tubes in the tube bundle. A_{HT} is the heat transfer area, or the wetted area of the tube and fin surface. P_l is the longitudinal tube pitch. The Reynolds number is calculated from the hydraulic diameter as

$$Re_{D_h} = \frac{u_{max} D_h}{\nu} \tag{1.13}$$

with u_{max} being the maximum fluid velocity in the tube bundle [12]. This velocity can be estimated as a function of the tube bundle geometry, but for the purposes of this study it is assumed to be the same as the free stream velocity.

Biery et al. [13] proposed a transformation method of the correlation presented by Kays and London for triangular pitched tube banks to extend the correlation to different triangular pitch tube bank geometries. The original correlation was only valid for a small range of transverse and longitudinal tube pitches, and so Biery et al. developed a transformation method to predict C_h, the coefficient in the Kays and London correlation [12], based on geometric parameters of the tube bank. Biery found that the transformation method was broadly applicable to a large range triangular pitched tube bank configurations, and could be used to predict heat transfer coefficients to within 15% of experimental results.

Krishna et al. [5] developed highly accurate and versatile correlations for bare, disc finned, and cylindrical pin finned tube bundles. The researchers in this study conducted multivariate regression analysis on data sets from computational fluid dynamics (CFD) and existing literature to develop correlations for quantifying shell-side heat transfer and friction characteristics. Three sets of correlations for predicting performance, which include unified correlations for all geometries and two sets of more accurate geometry-specific correlations, are presented. The correlations predict the thermohydraulic performance of 90% of existing experimental and CFD data to within 15%. All of the correlations express the Colburn factor (j_H) and friction factor as a function of the Reynolds number and the geometric parameters of the tube and tube bank. For the purposes of this study, the unified correlations are used because they are validated for the selected tube geometry [5, 14].

$$j_H = 0.47 \frac{D_h}{D_E}^{0.53} \frac{P_t}{D_t}^{-0.21} \frac{P_l}{D_t}^{-0.19} \frac{D_f}{D_t}^{0.12} \frac{S-\delta_f}{S}^{-0.38} Re_{D_h}^{-0.23} \tag{1.14}$$

where D_E is the effective diameter defined as the volume averaged diameter of the tube as if the fins were melted onto the tube surface evenly. P_t and P_l are the transverse and longitudinal tube pitch, respectively. The Colburn factor can be used to calculate the heat transfer coefficient by

$$h_{corr} = j_H Re_{D_h} Pr^{0.33} \frac{k}{D_h} \tag{1.15}$$

Krishna et al. make use of the geometric parameters described by the previously discussed papers. For their correlations, the fin efficiency is taken into account by reducing the effective heat transfer area A_{ht}, given by

$$A_{ht} = \eta_f N_f A_f + A_b \tag{1.16}$$

where N_f is the number of fins, A_f is the area of a single fin, and A_b is the area of the exposed base.

CHAPTER 2

Methods

2.1 Experimental Methods

2.1.1 Experimental Setup

The experimental work in this study was conducted using the UCLA Nano Transport Research Group's supercritical CO_2 test system that was constructed as part of the STHX correlation study by Krishna et al. The system is capable of producing sCO_2 flow at up to 25 grams per second at various temperatures and at a pressure of 100 bar. The key operating parameters and the piping and instrumentation diagram (P&ID) of the sCO_2 system fabricated by Accudyne Systems, Inc. is shown in Table 2.1 and Figure 2.1.

sCO2 Temperature Range	RT-300°C	**sCO2 Operating Pressure**	100 bar
sCO2 Max Flow Rate	25 g/s	**Air Temperature Range**	RT-400°C
Air Operating Pressure	30 psi	**Air Max Flow Rate**	10 g/s

Table 2.1: Experimental system operating parameters.

The experimental system also consists of an air supply and a 7.5 kW water-cooled chiller. The chiller was used to cool the return sCO2 from the test part. The pressurized air is fed from building air at ambient temperature and a separate air compressor, and can reach up to 300°C when the air heater is used. For this study, the air was used as the internal (tube-side) flow fluid. The entire experimental setup is shown in Figure 2.2.

The test parts consist of the tube (bare or finned) surrounded by a duct with a rectangular cross-section. The tube outer diameter was chosen to be 6.35 mm for consistency with the

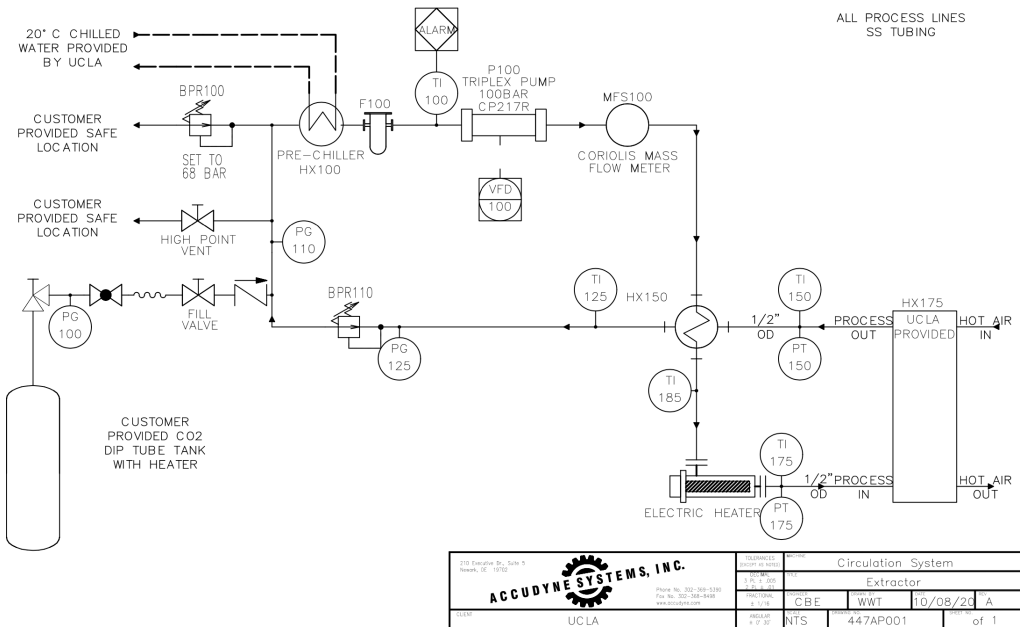

Figure 2.1: sCO_2 System piping and instrumentation diagram.

work conducted by Krishna et al., and to use as small of tubes as possible while still being able to fabricate the part at UCLA with standard welding practices. Smaller tubes are more likely to be used in highly compact heat exchangers because they allow higher heat transfer area per volume. By representing the results in terms of non-dimensionalized variables (i.e. Reynolds number and Nusselt number), the designs are still able to be compared to results from previous studies independent of geometry.

The duct surrounding the tube was designed with the goal of achieving high Reynolds numbers of above 7,000 at the maximum CO_2 flow rate. As the mass flow rate of the external (sCO_2) flow was limited to 20-25 g/s, the duct cross sectional area was fixed to achieve the target Re over bare tubes for the highest external flow temperature case. A simple, 2D CFD model was developed to evaluate the effect of duct height on the heat transfer performance, with the goal being to minimize the effect of the duct's top and bottom walls on the flow around the tube. It was found that for a duct height greater than four times the tube outer diameter, the duct height did not affect the heat transfer performance of the tube. Therefore,

Figure 2.2: sCO_2 experimental system with installed test part.

the duct height was chosen to be 31.75 mm, and the duct width was chosen to be 26.96 mm. The width was chosen such that there was space for 8 fins on the tube with a fin pitch of 3.175 mm and a Reynolds number of just over 7,000 could be achieved for a mass flow rate of 25 g/s. There is a distance of 1.5875 mm between the first and last fins and the duct walls, such that there is consistent spacing between each fin. Finally, the duct length was chosen to be 254 mm to allow for development of the turbulent flow profile before contacting the tube, while still fitting inside of the experimental system and the machines used for fabrication.

Two fin geometries were used in this study – disc and parabolic fins. Disc fins are the simplest type of annular fins and are thought to be the least expensive to fabricate due to their simplicity. Parabolic fins have been shown to have the highest theoretical fin efficiency of any annular fin and have a lower friction factor than disc fins, but they are generally more

expensive to fabricate due to the more complex machining process. However, as shown in Table 2.2 below, the parabolic fins have significantly lower volume (V) than the disc fins while providing a comparable increase in heat transfer surface area (SA). This provides the benefit of a lower system weight and lower material costs to fabricate the finned tubes. The fin diameter ($D_f = 12.7$ mm), fin pitch ($S = 3.175$ mm), and base thickness ($\delta_{fb} = 1.5875$ mm) are equal in both fin geometries. For the parabolic fins, the fin tip thickness is 0.508 mm. The final tube designs are shown in Figures 2.3 and 2.4 below.

Geometry	SA Added Per Fin (m^2)	Total SA	V Added Per Fin (m^3)	Total V
Bare	N/A	5.3838×10^{-4}	N/A	5.4635×10^{-7}
Disc	2.214×10^{-4}	2.31×10^{-3}	1.5083×10^{-7}	1.7530×10^{-6}
Parabolic	1.8162×10^{-4}	1.99×10^{-3}	7.6753×10^{-8}	1.1604×10^{-6}

Table 2.2: Surface area (SA) and volume (V) added by each fin and for the tube in total.

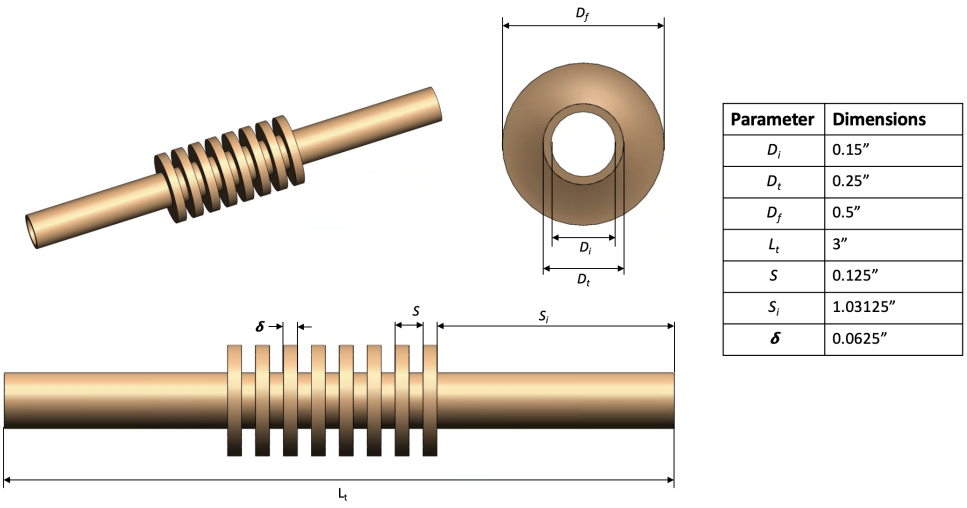

Figure 2.3: Dimensions of the disc-finned tube.

The finned tubes were manufactured by Mumford Micro Machine Works, LLC and were machined from a single piece of Haynes-282, so there is no thermal contact resistance between the tube and fins. The rest of the duct is Inconel-625, which is similar enough in composition to Haynes-282 that they can be welded together. A waterjet cutter was used to cut the

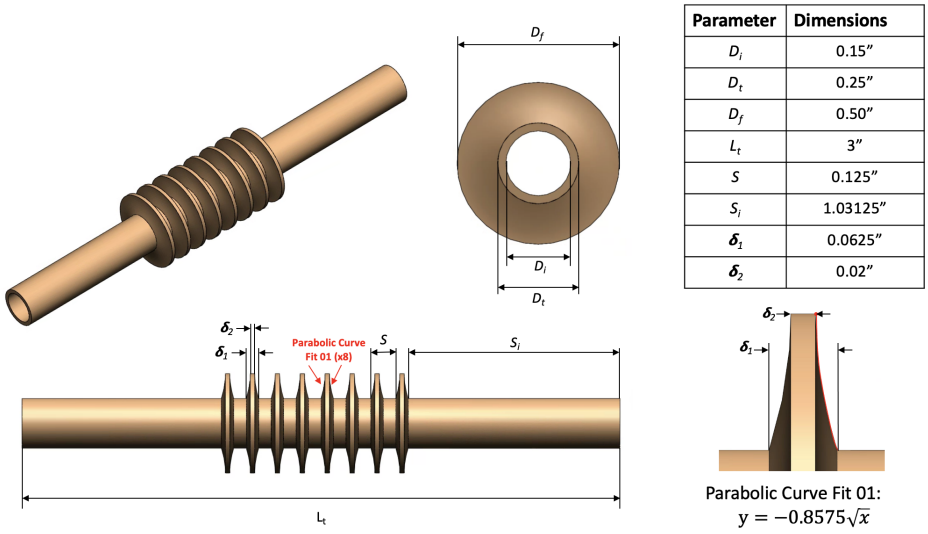

Parameter	Dimensions
D_i	0.15″
D_t	0.25″
D_f	0.50″
L_t	3″
S	0.125″
S_i	1.03125″
δ_1	0.0625″
δ_2	0.02″

Figure 2.4: Dimensions of parabolic-finned tube.

Inconel sheets into 6 rectangular faces, and the parts were welded such that the welds are on the exterior of the duct. The welding of the final test parts was done at UCLA with Inconel-625 weld filler. The tubes at the inlet and outlet of the shell and tube are connected to the sCO_2 system with Yor-Lok tube fittings as shown in Figure 2.5. All in-line instrumentation is connected to the test part by Yor-Lok fittings as well. The connections to the system are shown in Figure 2.6.

Temperature was measured by K-type thermocouples at six points in the test part: two in the external flow upstream of the tube, two in the external flow downstream of the tube, one at the internal flow inlet, and one at the internal flow outlet. Temperature samples were taken at a rate of one sample per second and recorded by a National Instruments DAQ. After initial testing, it was found that the temperature difference measured in the external flow was very small compared to the flow temperature, and was typically within the measurement error of 0.75% provided by the thermocouple manufacturer. Therefore, only the air inlet and outlet temperatures and the average of the inlet sCO_2 measurements are used in the analysis and results. Pressure is measured by analog pressure gauges at the internal flow inlet and

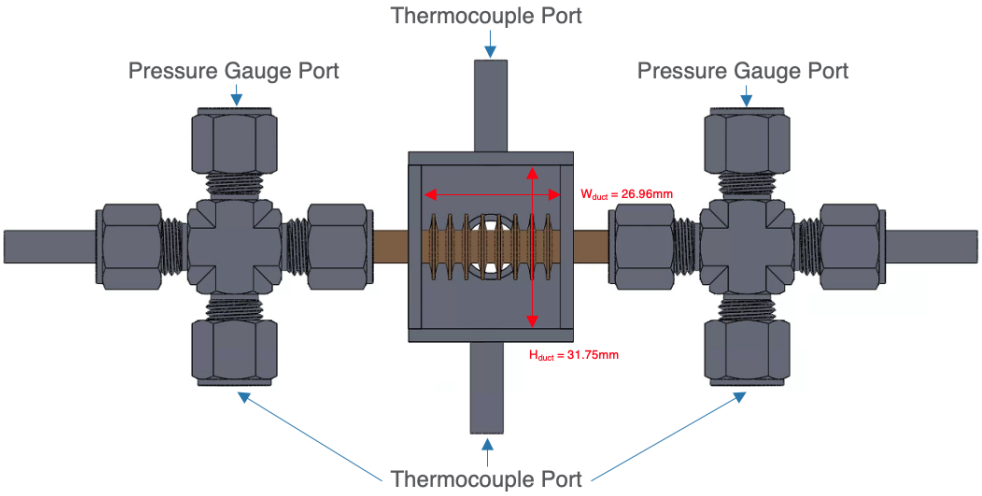

Figure 2.5: CAD drawing of the duct and tube with Yor-lok fittings

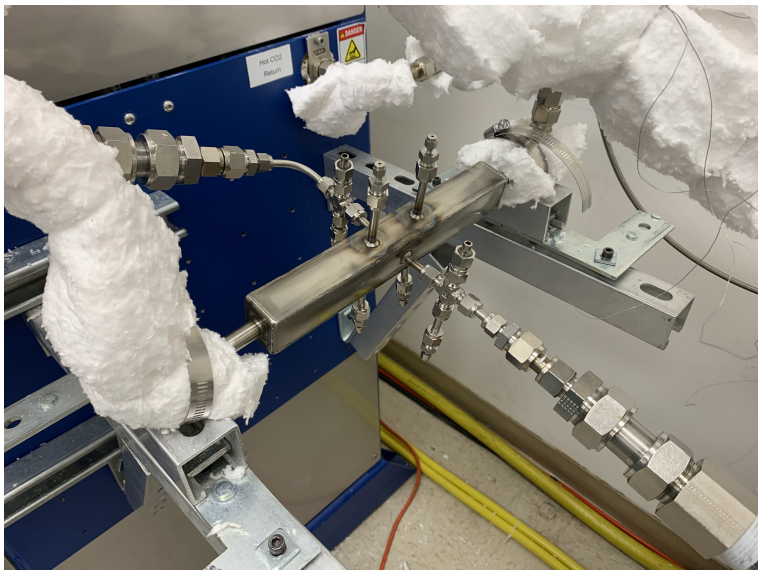

Figure 2.6: Test part installed in the sCO_2 system

outlet. For the external flow, pressure is measured at the sCO_2 system outlet, and was maintained at 100 bar throughout testing. It was not feasible to measure pressure inside of the test part due to the high operating temperature and pressure. Measuring surface temperatures of the tube was determined to be too challenging to do without disturbing the external

flow around the tube. The diameter of the thermocouples is 1.5875 mm, which is a quarter of the tube diameter, so placing thermocouples on the tube surface would affect the heat transfer performance significantly. Previous studies, such as Watel et al. [17], attempted to measure surface temperatures using non-contact methods such as infrared thermography that could be applied in future studies.

2.1.2 Safety and Procedures

Several physical safety measures were put in place for operating the experimental system. Before each test part was installed in the sCO_2 loop, burst pressure testing was conducted using a manual hydrostatic pressure tester. Each part was tested at 150% of the operating pressure of 100 bar as an added safety factor. Additionally, a plexiglass shield was installed in front of the exposed process tubes to protect from any potential hazards. All tubing that is outside of the process equipment is covered in ceramic insulation to prevent heat loss from the experimental system and to prevent burns. Safety goggles and a lab coat were required to operate the system. Safety measures were also implemented as part of the experimental procedure, and are discussed in the procedure.

For each tube geometry (bare tube, disc-finned, and parabolic-finned), the experimental procedure was designed to test the tubes at a variety of external flow Re and temperatures. The external mass flow rate could only be controlled by changing the sCO_2 compressor speed, and so the test cases are based on those speeds instead of mass flow rates. The flow rate of the internal flow was also varied in this study in order to achieve a wider range of tube surface temperatures. The experimental procedure, which includes much of the system startup procedure developed by Krishna et al., was as follows:

1. Check that there are no loose fittings in the CO_2 or air loops by manually attempting to loosen the fittings. If any fittings are loose, re-tighten them using two wrenches.

2. Open the chilled water supply and return valves to provide flow to the chiller. Turn on the chiller and lower the temperature setpoint in increments of 2°C until the chiller temperature reaches 5°C. Check that the sCO_2 system is receiving a coolant flow rate of at least 4 gallons per minute indicated by the float on the front of the sCO_2 system.

3. Charge the sCO_2 system by opening the CO_2 cylinder and the system fill valve until the pressure stops rising. Vent the system to remove any air that may have entered the system by closing the fill valve and opening the high point vent valve until the system pressure has dropped to 300 psi. Refill the system by closing the vent valve and re-opening the fill valve.

4. After the system is charged with CO_2, leave the CO_2 cylinder and the fill valve open and start the sCO_2 compressor at 25% speedby using the sCO_2 system HMI. Check that the flow rate is between 10-12 g/s.

5. Open the building air supply, and set the flow rate to 2.5 g/s by using the AliCat flow control valve serial monitor.

6. Set the sCO_2 heater to 100°C by using the sCO_2 system HMI. Wait until the temperature is steady.

7. Start recording data by starting the LabView module.

8. Once the system reaches steady state (all measured temperatures fluctuate by less than 1% over a period of 5 minutes), record the timestamp, the current high and low sCO_2 mass flow rate, and air inlet and outlet pressures. The timestamp is to ensure that the temperature data can be matched with the manually recorded information at each test case. The high and low mass flow rates are recorded because flow rate typically fluctuates between 1-5% even at steady state.

9. Change all settings to those specified by the next test case and repeat the previous step until all test cases are exhausted. The test cases are summarized in Table 2.3.

Case #	Compressor SP (%)	sCO_2 T (°C)	Air Flow (g/s)	**Case #**	Compressor SP (%)	sCO_2 T (°C)	Air Flow (g/s)
1	25	100	2.5	**33**	25	100	5
2	30	100	2.5	**34**	30	100	5
3	35	100	2.5	**35**	35	100	5
4	40	100	2.5	**36**	40	100	5
5	45	100	2.5	**37**	45	100	5
6	50	100	2.5	**38**	50	100	5
7	55	100	2.5	**39**	55	100	5
8	60	100	2.5	**40**	60	100	5
9	25	150	2.5	**41**	25	150	5
10	30	150	2.5	**42**	30	150	5
11	35	150	2.5	**43**	35	150	5
12	40	150	2.5	**44**	40	150	5
13	45	150	2.5	**45**	45	150	5
14	50	150	2.5	**46**	50	150	5
15	55	150	2.5	**47**	55	150	5
16	60	150	2.5	**48**	60	150	5
17	25	200	2.5	**49**	25	200	5
18	30	200	2.5	**50**	30	200	5
19	35	200	2.5	**51**	35	200	5
20	40	200	2.5	**52**	40	200	5
21	45	200	2.5	**53**	45	200	5
22	50	200	2.5	**54**	50	200	5
23	55	200	2.5	**55**	55	200	5
24	60	200	2.5	**56**	60	200	5
25	25	250	2.5	**57**	25	250	5
26	30	250	2.5	**58**	30	250	5
27	35	250	2.5	**59**	35	250	5
28	40	250	2.5	**60**	40	250	5
29	45	250	2.5	**61**	45	250	5
30	50	250	2.5	**62**	50	250	5
31	55	250	2.5	**63**	55	250	5
32	60	250	2.5	**64**	60	250	5

Table 2.3: Test cases based on compressor set point (SP), external flow temperature, and internal flow rate.

10. Stop the data recording. Turn off the CO_2 heater and allow the system to run until the CO_2 temperature indicated on the system HMI is under 50°C.

11. Turn off the sCO_2 compressor, chiller, and air supply valve. Shut the chilled water supply and return valves. Close the sCO_2 system fill valve and the CO_2 cylinder.

2.1.3 Data Analysis

The raw temperature data recorded on the DAQ were first processed to extract steady state air inlet and outlet temperatures. Steady state conditions were verified by analyzing the 30-second average following the time stamp recorded during the experiment. The steady state air inlet and outlet temperature and pressure data were used to determine the total heat transfer rate (q_r) for each test case. The specific enthalpies (h_{in} and h_{out}) of air at the inlet and outlet were calculated using the CoolProp fluid properties database [15] at the recorded temperatures and pressures. The overall rate of heat transfer is given by

$$q_r = \dot{m}_{air}(h_{in} - h_{out}) \tag{2.1}$$

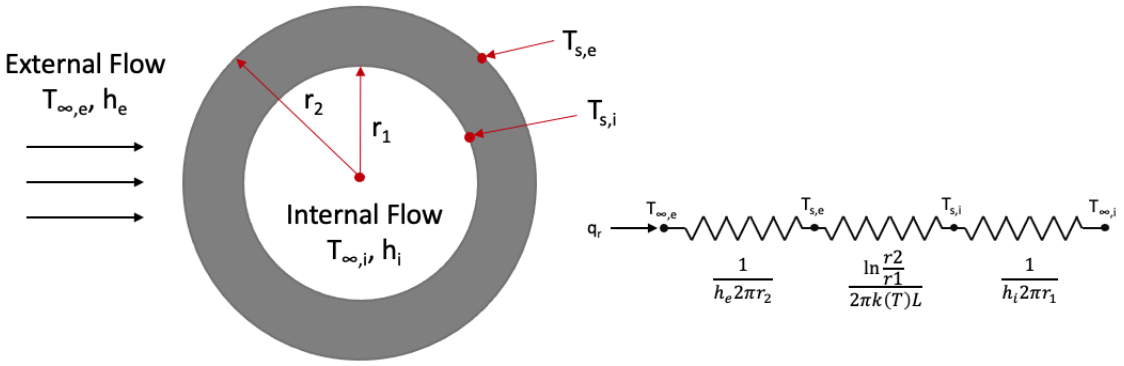

Figure 2.7: Thermal circuit representation of a bare tube in cross-flow.

The system was analyzed as a thermal circuit with known heat transfer rate (q_r) and mean fluid temperatures. This model, depicted in Figure 2.7, makes several key assumptions: (1) the heat transfer rate is uniform and constant through the tube in the radial direction, (2) the fluid properties are constant and the properties of air are well estimated by the mean temperature and pressure, (3) all heat transfer into the internal fluid is from convection by the external fluid to the tube surface (i.e. the system is well insulated, and conduction from the duct walls and radiation are negligible), (4) the internal and external flow are

fully developed turbulent flow, (5) the thermal conductivity of Haynes-282 is uniform and a function of temperature only, (6) and that the fin surfaces have the same heat transfer coefficient as the bare tube when calculating fin efficiency. Because surface temperatures of the tubes were not measured, the system could not be solved without estimating the internal heat transfer coefficient (h_i). The Dittus-Boelter correlations for turbulent flow in circular tubes are used to estimate h_i based on the internal flow conditions and the tube geometry. Although this correlation can introduce error of up to 25% depending on the conditions, it compares closely to most other correlations for tube flow [16].

$$Nu_D = 0.023 Re_D^{\frac{4}{5}} Pr^n \tag{2.2}$$

where n = 0.4 for heating (the surface is at a higher temperature than the internal fluid). The tube surface temperatures were found using the thermal circuit for radial conduction. The temperature dependent thermal conductivity of Haynes-282 (k_{Haynes}) was accounted for by assuming constant k_{Haynes} for shells of thickness dr. The conduction equation was solved for each shell to find the shell surface temperatures using k_{Haynes} calculated by linear interpolation with the thermal conductivity data provided by the material manufacturer. For this study, 100 shells of constant thickness were used as it was found that the change in predicted surface temperature was negligible with additional divisions of the tube volume. The external heat transfer coefficient (h_e) and the Nusselt number were then found using the external flow properties and the predicted tube outer surface temperature [17].

$$q_r = \frac{1}{h_e 2\pi r_2}(T_{\infty,e} - T_{s,e}) \tag{2.3}$$

$$q_r = \frac{ln(r2/r1)}{2\pi k_{Haynes}(T) L}(T_{s,e} - T_{s,i}) \tag{2.4}$$

$$q_r = \frac{1}{h_i 2\pi r_1} \tag{2.5}$$

The fin efficiencies were also calculated from the experimental data. By using the bare tube data to obtain the tube outer surface temperature (or base temperature, T_b) and the

base heat transfer coefficient (h_e) at a given Re, the maximum heat transfer rate of each finned tube design could be predicted. In this scenario, the heat transfer coefficient of the fins is assumed to be the same as for the bare tube at all locations. The fin efficiency is then given by

$$q_r = N_f \eta_f h_e A_f (T_b - T_\infty, e) + h_e A_b (T_b - T_{\infty,e}) \tag{2.6}$$

where A_f is the area of the fins and A_b is the area of the exposed base (bare tube surface) [17].

This study also used single tube and tube bundle correlations for Nusselt number to compare to the experimental results. The single tube correlations were developed by Chen et al. and Watel et al., and the tube bundle correlation was developed by Krishna et al. The single tube correlations directly predict the Nusselt number based on the system geometry and the Reynolds number. The tube bundle correlation predicts the Colburn factor, from which the Nusselt number can be derived, from the tube bundle geometry and the Reynolds number. In order to compare the tube bundle correlations with the experimental results, this study assumes a tube bundle configuration with the maximum tube pitch in each direction. This is meant to most accurately correspond to the single tube case. For the unified correlations presented by Krishna et al., the maximum pitch ratios in the transverse (P_t) and longitudinal (P_l) directions are $\frac{P_t}{D_{ot}} = 3.5$ and $\frac{P_l}{D_{ot}} = 6$.

A correlation for fin efficiency as a function of tube geometry and Reynolds number, developed by Chen et al., is also presented alongside the experimental results. Finally, the fin efficiency can be solved analytically by assuming the average heat transfer coefficient on the fins and the surface temperature of the exposed bare tube.

CHAPTER 3

Results and Discussion

3.1 Experimental Results

Data was collected and analyzed for the bare tube, disc finned tube, and parabolic finned tube designs in three separate experiments. The results comparing the heat transfer performance of the three designs are presented in Figure 3.1 for each of the different external flow temperatures and internal mass flow rates as the Nusselt number (Nu) versus the Reynolds number. As expected, the Nusselt numbers of the finned tube designs are generally much higher (typically greater than twice) the Nu of the bare tube. The disc-finned tube consistently out-performed both the bare tube and the parabolic-finned tube in terms of overall heat transfer. However, the performance of the parabolic- and disc-finned tubes was very close for most cases. This result is somewhat expected as well, considering that the overall heat transfer surface area of the disc-finned design is 16% higher than that of the parabolic-finned design.

Although the general trends and relative heat transfer performance compared well to expectations, the calculated Nusselt numbers for the cases with an internal flow rate of 2.5 g/s are much higher than the values expected from related studies. The total heat transfer rates for these cases were slightly lower than those of the 5 g/s cases, so the much higher Nu may be explained as a product of the analysis method for estimating tube surface temperatures. The temperature difference between the outer tube surface and the sCO_2 flow predicted by the thermal circuit model for the 2.5 g/s air flow scenario is 4-5 times larger

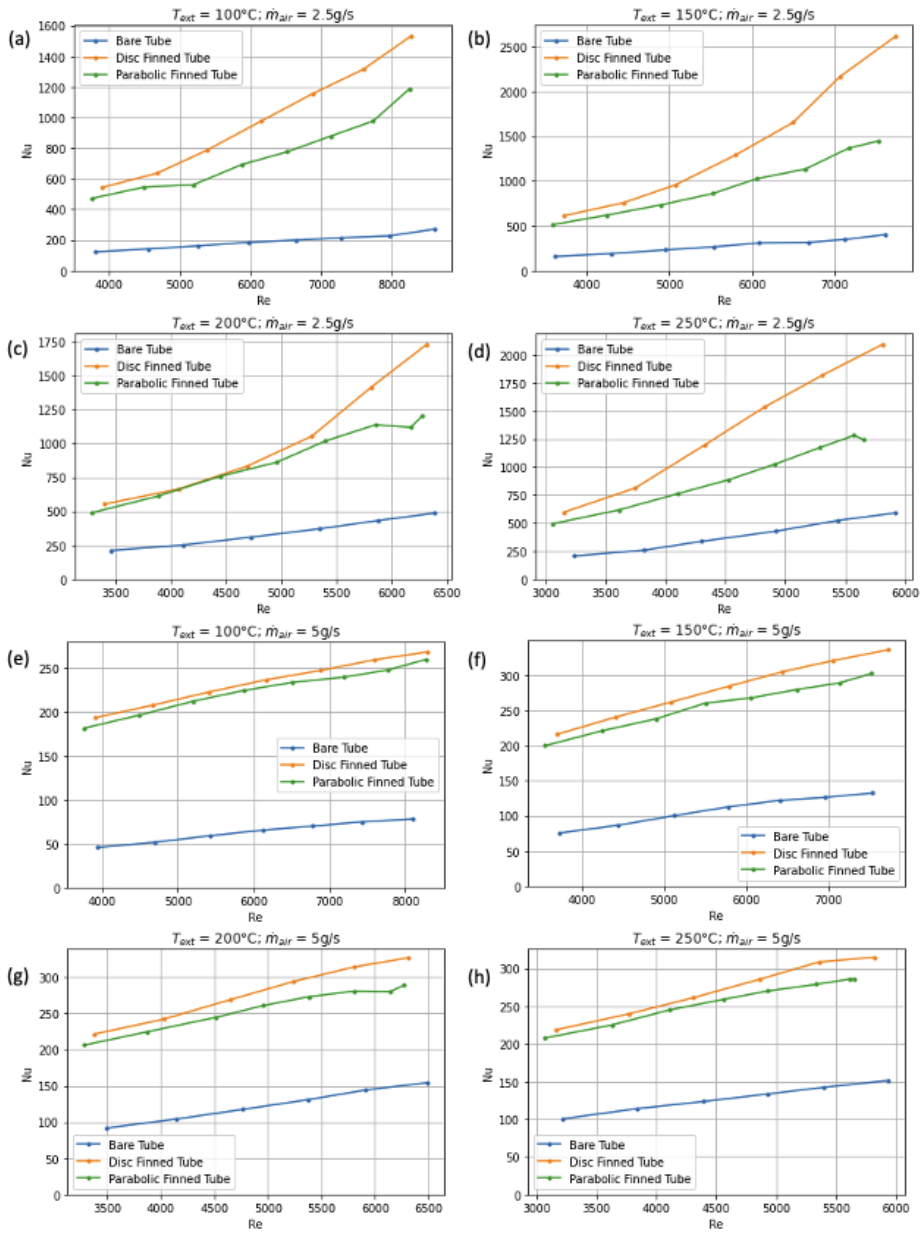

Figure 3.1: Experimental results of Nu vs. Re for each of the tube designs. Plots (a)-(d) have external flow temperatures of 100, 150, 200, and 250°C respectively and all have an internal flow rate of 2.5 g/s. Plots (e)-(h) have external flow temperatures of 100, 150, 200, and 250°C respectively and all have an internal flow rate of 5 g/s.

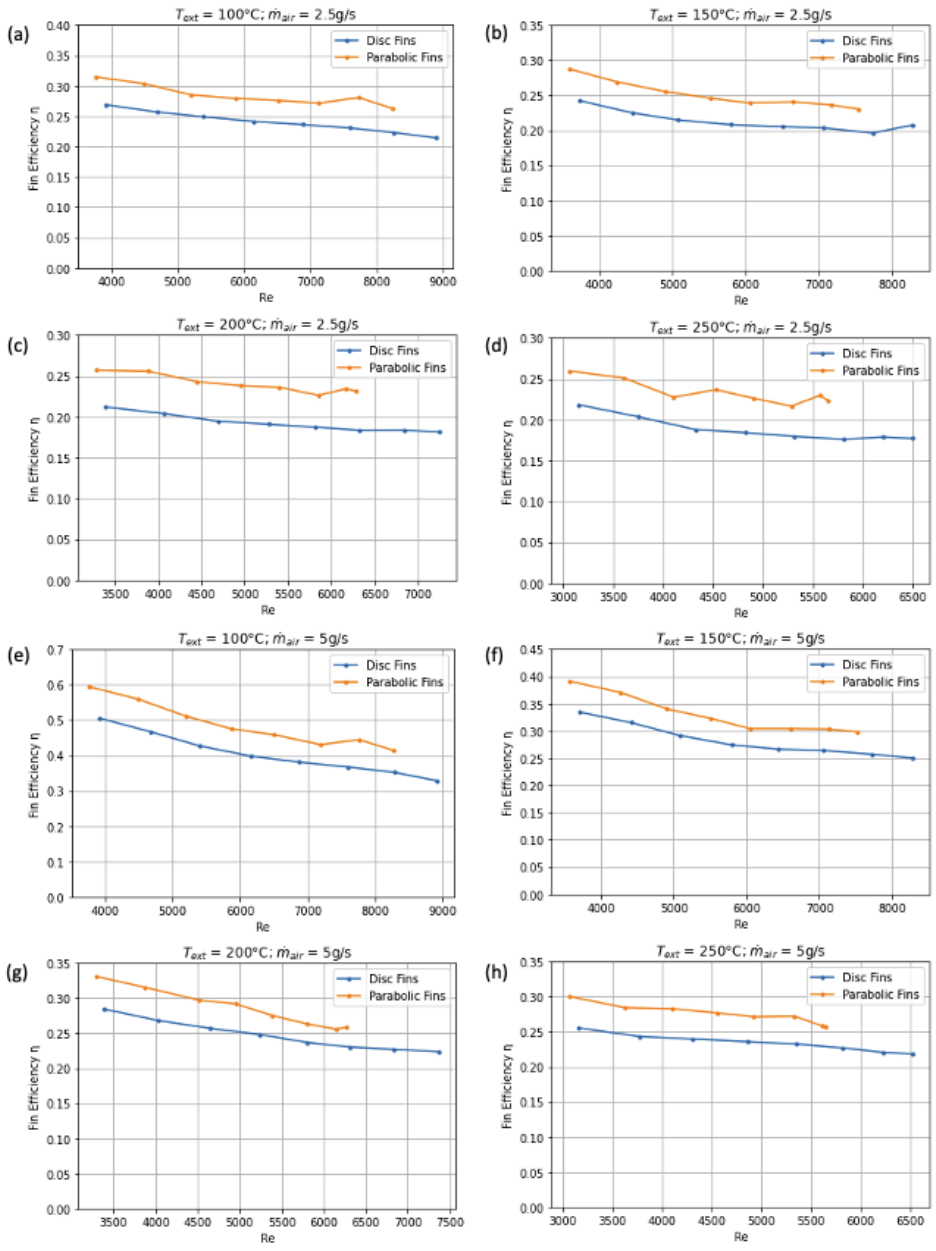

Figure 3.2: Experimental results of fin efficiency vs. *Re* for disc and parabolic fin geometries. Plots (a)-(d) have external flow temperatures of 100, 150, 200, and 250°C respectively and all have an internal flow rate of 2.5 g/s. Plots (e)-(h) have external flow temperatures of 100, 150, 200, and 250°C respectively and all have an internal flow rate of 5 g/s.

than that of the 5 g/s air flow scenarios. These unexpected results may be caused by either an incorrect estimation of the internal heat transfer coefficient, or by other limitations of the experimental system. If the internal heat transfer coefficient is underestimated for the lower Re internal flow, it means that the tube surface temperature is assumed to be much higher than it actually is and the external heat transfer coefficient will be overestimated.

Another, more likely explanation for the Nusselt number results in the 2.5 g/s air flow cases is that the measured heat transfer is not purely from convective heat transfer within the duct as the model assumes. It is likely that a significant source of error is due to conduction through the welded joints between the tube and the duct walls, as there is additional length before and after the duct where the tube walls are heated and are transferring heat to the internal flow. This means that there is additional heat transfer to the air before temperature is measured, which the model treats as convection from the external flow. The test parts were designed to minimize the length of tube between the duct walls and thermocouples, but there is still extra tube length to accommodate the four-way tube fittings into which the thermocouples are installed. This excess length would have a lower surface temperature as distance from the duct increases, so this effect should be relatively small. In the 5 g/s internal flow scenarios, this additional heat transfer length may not be as significant relative to total heat transfer since the heat transfer within the duct is larger. However, without additional measurements of tube surface temperature, it is difficult to quantify the effect of conduction to the tube from the duct walls.

The fin efficiencies were also calculated for each fin geometry and are presented in Figure 3.2 as a function of Re. The bare tube data was used as a baseline to calculate the efficiency of each of the finned tubes. The experimental results show that fin efficiency decreases with increasing Re, and that the parabolic fins have a consistently higher fin efficiency than the disc fins. These results are consistent with what is expected based on previous studies by Chen et al. and Hu et al. The parabolic fins are 5-10% more efficient than the disc tubes for all cases, which is also expected. For parabolic fins, efficiency is higher because there is

less surface area on the fin tip where the surface temperature would be the highest. The results also show that fin efficiency is somewhat dependent on the internal flow rate and the external flow temperature. The fin efficiency of both geometries in the case with an external flow temperature of 100°C and an internal flow rate of 5 g/s is especially high. This can be attributed to the low heat transfer rates and external heat transfer coefficients calculated for the bare tube case at lower values of Re.

3.2 Comparison to Reference Correlations

The experimental results were also compared with the previously discussed correlations for Nusselt number. Figure 3.3 shows the experimental results for Nu alongside the predicted values of Nu from the correlations by Chen et al., Watel et al., and Krishna et al. Only the experimental data for disc fins are presented because the correlations are not validated for parabolic fin geometries. As evident in Figure 3.3, the experimental results do not compare well with the correlations. The experimental results consistently overpredict the Nusselt number which may be attributed to the limits of the analysis as discussed in Section 3.3. The results do, however, follow the same trends as the correlation where Nu is almost linearly correlated with Re. The correlations agree fairly well to each other, but Watel et al.'s correlation predicts Nu to be higher than the other two correlations.

Chen et al. also proposed a correlation for fin efficiency of disc fins as a function of of the fin geometry and Reynolds number. The predicted fin efficiencies from this correlation, the analytical solution of fin efficiency, and the experimental results are presented in Figure 3.4. The experimental data compares favorably to Chen et al.'s correlation, especially for the case with 150°C external flow temperature. For higher temperatures, the correlation overestimates the observed fin efficiency. Chen et al.'s correlation is only a function of the Reynolds number and the fin geometry, so the differences between different external and internal flow conditions do not affect the predictions of η_f.

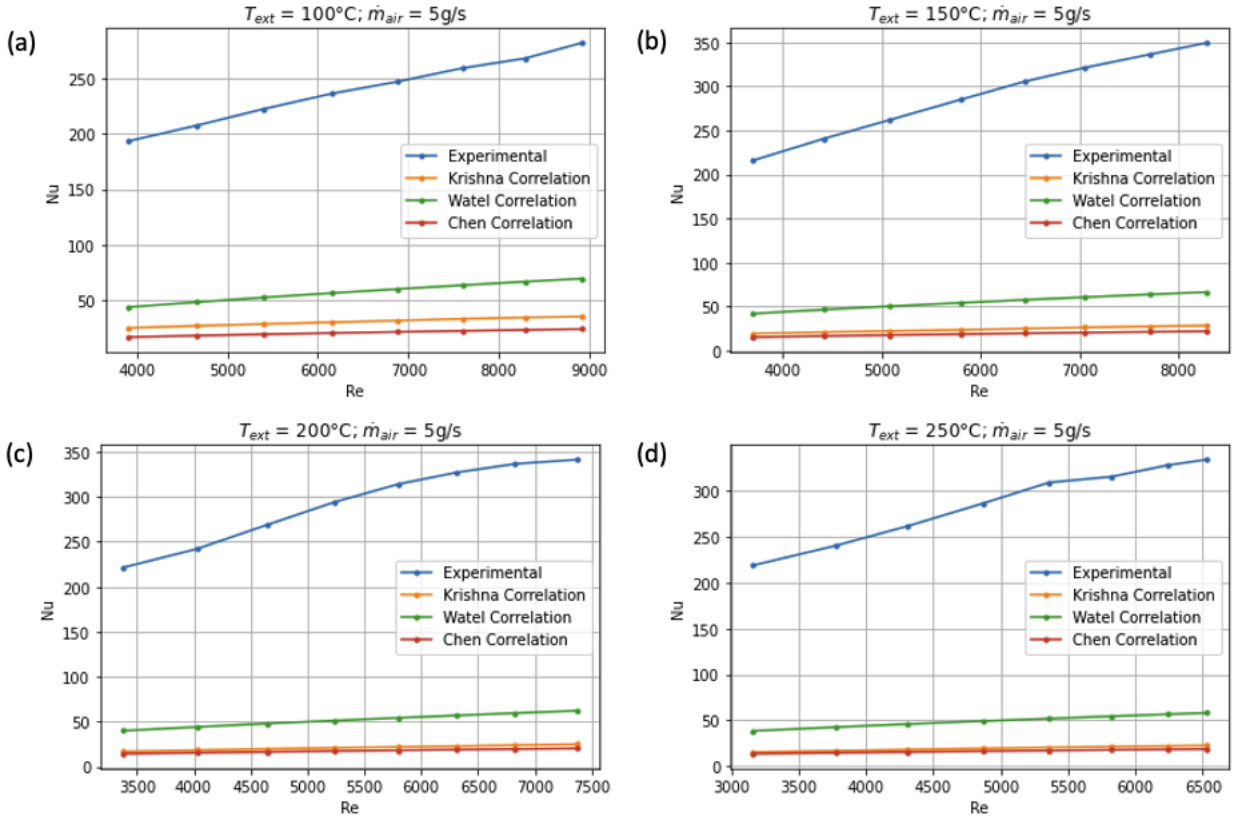

Figure 3.3: Comparison of Nu vs. Re from experimental results and correlations for the disc-finned tube. The data is presented for experimental cases with internal flow rates of 5 g/s and external flow temperatures of (a) T_{ext}=100°C, (b) T_{ext}=150°C, (c) T_{ext}=200°C, (d) T_{ext}=250°C.

3.3 Experimental Error

Although the experimental results follow the expected trends described in the literature, there are several sources of potential error in the results. The first source of error is measurement uncertainty. As previously mentioned, the sensor error of the K-type thermocouples is ±0.75% of the measured value. For the air inlet and outlet temperatures, this error is very small as the highest measured temperature is less than 50°C. For the sCO_2 measurements, the average of the two measurements is taken and so the error in the average is about

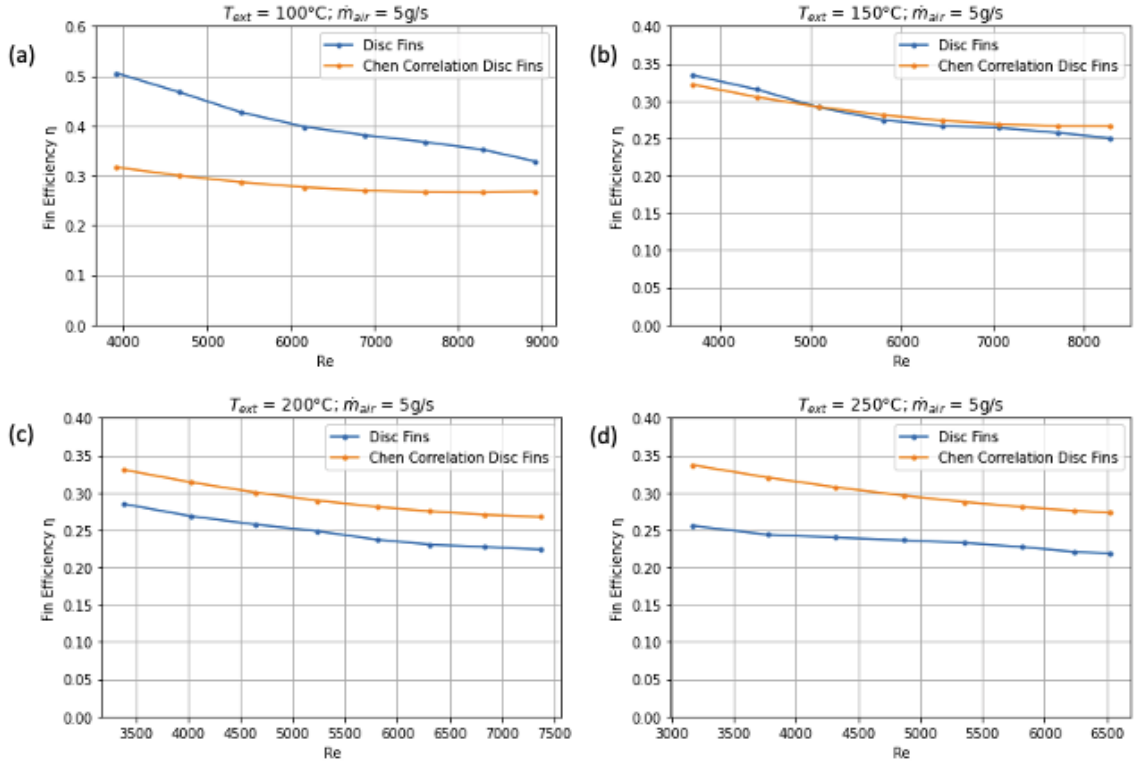

Figure 3.4: Comparison of fin efficiency vs. *Re* from experimental results and Chen et al.'s correlation for the disc-finned tube. The data is presented for experimental cases with internal flow rates of 5 g/s and external flow temperatures of (a) T_{ext}=100°C, (b) T_{ext}=150°C, (c) T_{ext}=200°C, (d) T_{ext}=250°C.

±0.53%. At the highest temperature case, this amounts to a 1.25°C expected error. The air inlet and outlet pressure is measured by analog gauges with demarcations of 0.5 psi, and so the reading error is expected to dominate the total error of the air pressure measurements and can be estimated at ±0.25 psi. The air flow controller has an uncertainty of 0.01 g/s which is expected to be negligible compared to other sources of measurement error. The sCO_2 flow rate monitor fluctuates during steady state measurements, and this dominates the overall error of the flow measurement. Typically, the flow rate fluctuates by about ±1%, but can be up to ±5% for specific cases.

Another source of error is that the analysis method for producing experimental results is limited by several key assumptions. The model assumes that the fluid properties for internal and external flow are constant for calculating Reynolds number and density, and are approximated by using the mean values for pressure and temperature. This is typically a reasonable assumption at the relatively low differences in measured temperature and pressure. Another key assumption is the use of the Dittus-Boelter correlation for predicting the average heat transfer coefficient in the internal flow. As noted in the literature, this correlation can differ from actual results by up to 25% in certain cases and often overestimates the heat transfer coefficient as compared to other correlations. Without additional instrumentation to measure surface temperatures, there is no way to exactly quantify the error attributed to this assumption. However, since this correlation tends to overestimate the internal heat transfer coefficient the effect on the Nusselt number would be lower than expected instead of higher, which is what was observed. The internal flow correlation is not expected to be the main cause of error. There are also aspects of the experimental system that are not captured by the model as well. First, the model assumes that there is no effect from radiative heat transfer from the duct walls to the tube surface. This is typically a reasonable assumption for the operating temperatures and considering that the gray-body emissivity of Inconel is less than 0.25 at these temperatures. However, it would account for some of the heat transferred to the air and reduce the calculated heat transfer coefficient.

The main source of error is likely due to conduction heat transfer from the duct walls to the ends of the tube as previously discussed. This will cause the measured heat transfer to be higher than the actual heat transfer by convection inside of the duct because the tube is heated upstream and downstream of where the tube is welded to the duct. Since the duct walls are being heated by the sCO_2 flow, they are likely very close to the fluid temperature and will be constantly supplying heat to the tube. This effect is depicted in Figure 3.5.

It is very difficult to quantify the amount of additional energy supplied to the internal fluid by this mode of heat transfer due to several factors including the unknown thermal

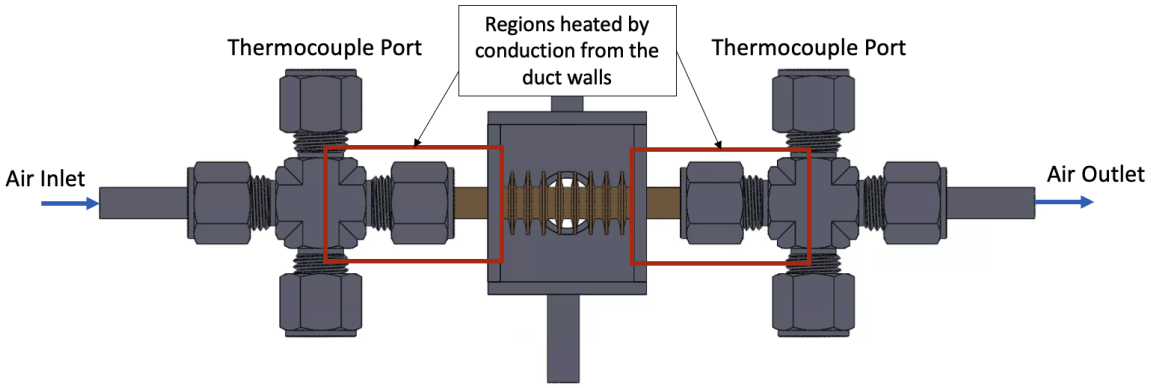

Figure 3.5: Depiction of conduction through the duct walls which likely contributes to experimental error.

conductivity of the welded interface, the unknown temperature profile of the tube outside of the duct, and the thermal properties of the tube fittings which have complicated geometries. The calculated Nusselt numbers vary from the correlations by 5-10 times in all of the 5 g/s cases, and the calculated Nusselt numbers are very sensitive to the measured temperature difference. When the measured temperature difference is artificially lowered by 55-65%, the results match very closely with Nu predicted by Watel et al.'s correlation for all of the 5 g/s cases. This suggests that a large portion of the measured heat transfer rate is due to this additional source of energy that is not accounted for by the model. The total distance (made up of tube and fitting) between the duct and the thermocouples is greater than the tube length inside of the duct, and so it is reasonable that this additional heated length may account for a large portion of the measured temperature difference.

In future studies, this source of error may be addressed by adding additional surface temperature measurements on the exterior of the tube just outside of the duct. This would provide some information that can be used to estimate how much heat is being transferred to the internal fluid by these regions. Surface temperature measurements on the finned tubes inside of the duct would be the ideal way to address the issue since the heat transfer coefficients could be directly calculated from those measurements. However, it is difficult to

attach instrumentation inside of the small duct without disrupting the flow profile around the tube and fins. The issue could also be addressed by shortening the length of tube in between the duct walls and the thermocouple ports, although this may require the test parts to be redesigned such that tube fittings are not used to hold the thermocouples.

CHAPTER 4

Conclusions

This study experimentally characterized the heat transfer performance of bare, disc-finned, and parabolic-finned tubes in supercritical CO_2 cross flow over a range of external flow conditions. The results are presented as Nusselt number versus Reynolds number and fin efficiency versus Reynolds number. They show that the disc and parabolic finned tubes greatly outperform bare tubes in terms of overall heat transfer, that the disc-finned tube consistently outperforms the parabolic fins in overall heat transfer coefficient, and that the parabolic fins are 5-10% more efficient than the disc fins in all cases. The relative performance of each tube design is represented well in this study. However, the results do not compare favorably with single tube and tube bank correlations for Nusselt number from previous studies. Several potential sources of deviation from these correlations are proposed in the discussion, and much of the error can likely be attributed to the assumptions made to account for a lack of measurements of the tube surface temperatures and the limitations of the experimental setup.

The results of this study show that finned tubes can vastly improve heat transfer effectiveness in shell and tube heat exchangers as compared to bare tubes, and also shows that the each fin geometry has key benefits in terms of cost and performance. The disc fins offer a greater increase in surface area and therefore a higher average heat transfer coefficient, while the parabolic fins offer higher fin efficiency and comparable heat transfer performance with 49% less volume added. The manufacturing technique for fabricating the finned tubes will determine the overall costs of each finned tube design. For example, if the finned tubes are

machined as a single part from bulk material, the lower volume of Haynes-282 in the parabolic design will not be a factor in overall cost because both designs will be machined from the same sized bulk material. The increased complexity of the parabolic fins may add extra wear on machine tools and require additional machining time. If additive manufacturing is used, the parabolic design will require less material and less manufacturing time. For brazed and bonded fins, the thermal contact resistance of the weld must be considered because it may significantly change the performance of the fins. Another consideration for deciding between fin geometries is the specific requirements of the end use. If the cost of the thermal energy source is high, then heat exchanger effectiveness, and therefore the higher Nusselt number, would be especially important. For situations such as for hybrid-electric aircraft propulsion, the weight of the heat exchangers is especially important and so a parabolic-finned tube design would be more beneficial.

There is still much work to be done to fully characterize the heat transfer performance of the proposed fin designs for use in STHXs. The obvious next step is to conduct similar experiments on bundles of finned tubes with the same fin geometries. By using tube bundles, the results from experiments will be more naturally comparable to the correlations developed by Krishna et al. and others. Tube bundle results for average heat transfer coefficient can then be used to predict the performance of STHXs using Krishna et al's model or other methods. As part of a tube bundle study, multiple geometries should be used such that fin pitch, tube pitch, and parabolic fin tip thickness are varied. This could be used to develop and validate correction factors to Krishna et al.'s correlations, which are currently validated for disc and pin fins, to account for parabolic fins. Future studies should als o consider new methods of measuring tube surface temperature to minimize the sources of error discussed in this paper. This could include simply attaching thermocouples to downstream tubes or using thermocouples to measure internal temperatures where the flow is less important to characterize. More complicated methods, such as infrared thermography, to measure surface temperature or using constant temperature heated cylinders in place of tubes, could also

be used to avoid disrupting the external flow around the fins. Aside from heat transfer performance, the pressure drop due to the tubes should be studied. The pressure drop will determine the overall efficiency of the heat exchanger since it directly affects the energy required for compression. The different fin geometries will have different friction factors, and further studies are needed to understand if the difference will significantly affect overall heat exchanger performance. Finally, a comprehensive cost study should be conducted in order to fully understand the trade-offs between the two fin designs. This would likely be part of a larger SHTX cost study with known end uses, where the heat transfer results of each design would be an input into the cost model. Ultimately, future studies could further validate the proposed finned tube geometries for their eventual use in shell and tube supercritical CO_2 heat exchangers.

References

[1] Yoonhan Ahn, Seong Jun Bae, Minseok Kim, Seong Kuk Cho, Seungjoon Baik, Jeong Ik Lee, and Jae Eun Cha. Review of supercritical co2 power cycle technology and current status of research and development. *Nuclear Engineering and Technology*, 47(6):647–661, 2015. ISSN 1738-5733. doi: https://doi.org/10.1016/j.net.2015.06.009.

[2] Yaping Liu, Ying Wang, and Diangui Huang. Supercritical co2 brayton cycle: A state-of-the-art review. *Energy*, 189:115900, 2019. ISSN 0360-5442. doi: https://doi.org/10.1016/j.energy.2019.115900.

[3] Andrew Brittan, Jacob Mahaffey, and Mark Anderson. The performance of haynes 282 and its weld in supercritical co2. *Materials Science and Engineering: A*, 759:770–777, 2019. ISSN 0921-5093. doi: https://doi.org/10.1016/j.msea.2019.05.080.

[4] *sCO2 Power Cycle Component Cost Correlations From DOE Data Spanning Multiple Scales and Applications*, volume Volume 9: Oil and Gas Applications; Supercritical CO2 Power Cycles; Wind Energy of *Turbo Expo: Power for Land, Sea, and Air*, 06 2019. doi: 10.1115/GT2019-90493. V009T38A008.

[5] Akshay Bharadwaj Krishna, Kaiyuan Jin, Portonovo S. Ayyaswamy, Ivan Catton, and Timothy S. Fisher. Modeling of Supercritical CO2 Shell-and-Tube Heat Exchangers Under Extreme Conditions. Part I: Correlation Development. *Journal of Heat Transfer*, 144(5), 03 2022. ISSN 0022-1481. doi: 10.1115/1.4053510. 051902.

[6] Han-Taw Chen and Wei-Lun Hsu. Estimation of heat-transfer characteristics on a vertical annular circular fin of finned-tube heat exchangers in forced convection. *International Journal of Heat and Mass Transfer*, 51(7):1920–1932, 2008. ISSN 0017-9310. doi: https://doi.org/10.1016/j.ijheatmasstransfer.2007.06.035.

[7] Barbara Watel, Souad Harmamd, and Bernard Desmet. Influence of flow velocity and

fin spacing on the forced convective heat transfer from an annular-finned tube. *JSME International Journal Series B*, 42(1):56–64, 1999. doi: 10.1299/jsmeb.42.56.

[8] X. Hu and A. M. Jacobi. Local Heat Transfer Behavior and Its Impact on a Single-Row, Annularly Finned Tube Heat Exchanger. *Journal of Heat Transfer*, 115(1):66–74, 02 1993. ISSN 0022-1481. doi: 10.1115/1.2910671.

[9] Vincent T. Morgan. The overall convective heat transfer from smooth circular cylinders. volume 11 of *Advances in Heat Transfer*, pages 199–264. Elsevier, 1975. doi: https://doi.org/10.1016/S0065-2717(08)70075-3.

[10] N. Nagarani, K. Mayilsamy, A. Murugesan, and G. Sathesh Kumar. Review of utilization of extended surfaces in heat transfer problems. *Renewable and Sustainable Energy Reviews*, 29:604–613, 2014. ISSN 1364-0321. doi: https://doi.org/10.1016/j.rser.2013.08.068.

[11] Thomas Perrotin and Denis Clodic. Fin efficiency calculation in enhanced fin-and-tube heat exchangers in dry conditions. In *Proc. Int. Congress of Refrigeration 2003*, 2003.

[12] W.M. Kays and Alexander Louis London. *Compact Heat Exchangers*. Krieger Publishing Company, 1998. ISBN 9781575240602.

[13] J. C. Biery. Prediction of Heat Transfer Coefficients in Gas Flow Normal to Finned and Smooth Tube Banks. *Journal of Heat Transfer*, 103(4):705–714, 11 1981. ISSN 0022-1481. doi: 10.1115/1.3244530.

[14] Akshay Bharadwaj Krishna, Kaiyuan Jin, Portonovo S. Ayyaswamy, Ivan Catton, and Timothy S. Fisher. Modeling of Supercritical CO2 Shell-and-Tube Heat Exchangers Under Extreme Conditions: Part II: Heat Exchanger Model. *Journal of Heat Transfer*, 144(5), 03 2022. ISSN 0022-1481. doi: 10.1115/1.4053511. 051903.

[15] Ian H. Bell, Jorrit Wronski, Sylvain Quoilin, and Vincent Lemort. Pure and pseudo-pure fluid thermophysical property evaluation and the open-source thermophysical property library coolprop. *Industrial & Engineering Chemistry Research*, 53(6):2498–2508, 2014. doi: 10.1021/ie4033999.

[16] Dawid Taler and Jan Taler. Simple heat transfer correlations for turbulent tube flow. *E3S Web Conf.*, 13:02008, 2017. doi: 10.1051/e3sconf/20171302008.

[17] T.L. Bergman, F.P. Incropera, D.P. DeWitt, and A.S. Lavine. *Fundamentals of Heat and Mass Transfer*. Wiley, 2011. ISBN 9780470501979.

[18] Han-Taw Chen and Wei-Lun Hsu. Estimation of heat transfer coefficient on the fin of annular-finned tube heat exchangers in natural convection for various fin spacings. *International Journal of Heat and Mass Transfer*, 50(9):1750–1761, 2007. ISSN 0017-9310. doi: https://doi.org/10.1016/j.ijheatmasstransfer.2006.10.021.

[19] A. Ullmann and H. Kalman. Efficiency and optimized dimensions of annular fins of different cross-section shapes. *International Journal of Heat and Mass Transfer*, 32(6): 1105–1110, 1989. ISSN 0017-9310. doi: https://doi.org/10.1016/0017-9310(89)90010-0.